JOURNAL OF AIRCRAFT
Vol. 30, No. 4, July–Aug. 1993

Aileron and Sideslip-Induced Unsteady Aerodynamic Modeling for Lateral Parameter Estimation

Jatinder Singh* and S. C. Raisinghani†
Indian Institute of Technology, Kanpur, India

Aileron inputs and sideslipping motion of an aircraft will give rise to a trailing vortex system that is a function of time. To account for such unsteady aerodynamic effects into the lateral equations of motion, a model is proposed based on a simple vortex system. The expressions for induced sidewash and downwash angles obtained for such vortex system are recast so that the resulting equations of motion can be used for parameter estimation. Maximum likelihood method in frequency domain is used to analyze simulated flight data of an example airplane to study the effects of inclusion and omission of unsteady aerodynamic modeling on estimated parameters. Sensitivity of the extracted parameters to different control input forms is shown to reduce with the inclusion of unsteady aerodynamics.

Nomenclature

a_v, a_t = lift curve slope of the vertical and horizontal tail
a_y = linear acceleration along y axis
b = wing span
Ci = cosine integral of variable $\int_{\infty}^{z} (\cos t/t)\, dt$
$C_{L_{\delta_a}}$ = aileron control derivative, $\partial C_L/\partial \delta_a$, (Ref. 8)
C_{L_t} = lift coefficient of horizontal tail
ΔC_{L_t} = indicial lift coefficient of horizontal tail
C_y = side-force coefficient of vertical tail
c = chord
Ei = exponential integral of variable $\int_{-\infty}^{x} (e^t/t)\, dt$
E_1 = exponential integral of variable $\int_{z}^{\infty} (e^{-t}/t)\, dt$
g = acceleration due to gravity
I_x, I_z = moment of inertia about X and Z axis
j = $\sqrt{-1}$
l_v, l = vertical and horizontal tail length
m = mass of the airplane
p, r = roll and yaw rate
Si = sine integral of variable $\int_{\infty}^{z} (\sin t/t)\, dt$
S_w, S_v, S_t = wing, vertical tail, and horizontal tail area
t, τ = time
u = freestream velocity
y, z = constants in indicial side force, Eq. (4)
$\bar{y}$ = distance from center of gravity to aerodynamic center of the left and right panels of the horizontal tail
z_v = vertical height of aerodynamic center of vertical tail from c.g. of the aircraft
α = angle of attack at the wing
α_δ = aileron deflection parameter, $\partial\alpha/\partial\delta_a$, (Ref. 8)
β = angle of sideslip
δ_a, δ_r = aileron and rudder deflection
$\Delta\varepsilon$ = indicial downwash angle
$\Delta\sigma_1$, $\Delta\sigma_2$ = indicial sidewash angles
Λ = wing sweep
ρ = density of air
ϕ = bank angle
ω = angular frequency
∞ = infinity

Subscripts
r = root
ss = steady-state value
t = horizontal tail
v = vertical tail
w = wing

Superscripts
$\cdot$ = derivative with respect to time
$\sim$ = Fourier transform
$\top$ = transpose of a matrix
$'$ = total derivatives, Eq. (17)
$''$ = equivalent derivatives

Introduction

THE last few years have witnessed increased efforts at the modeling of unsteady aerodynamics into aircraft equations of motion for parameter estimation. Based on simplified Weissinger's vortex model for wing,[1] unsteady aerodynamics has been modeled into equations of motion for estimating longitudinal[2,3] as well as lateral[4–6] parameters. Such modeling is expected to lead to increased confidence and high fidelity in parameter estimation.

In Ref. 6, a model for sideslipping airplane was proposed and shown to be more plausible and inherently consistent as compared to the one suggested by Wells et al.[7] In this article the study of Ref. 6 is extended in two ways: 1) the proposed vortex system of the sideslipping wing is slightly modified to account for the center trailing vortex being parallel to the tip trailing vortices, unlike the way it was taken along X axis in Ref. 6 (see Fig. 1 of Ref. 6 and Fig. 1a of present article; and 2) a model is suggested for unsteady aerodynamics due to trailing vortex pattern from aileron input (see Fig. 1b). The lateral equations of motion with unsteady effects due to sideslipping and aileron input are so recast in the frequency domain that they become amenable for parameter estimation. Maximum likelihood method is used for parameter extraction from simulated data for an example airplane to show the effect of unsteady aerodynamics on estimated parameters.

Modeling of Unsteady Aerodynamics

A simplified arrangement of vortex system for a sideslipping wing and a wing with deflected ailerons is shown in Figs. 1a and 1b, respectively. The vortex pattern of Fig. 1a is similar to that used in Ref. 6 except for the central vortex line being at an angle β with respect to the X axis, unlike it being along X axis in Ref. 6.

The vortex system of Fig. 1b for positive aileron deflection assumes a vortex pattern for each panel of the wing due to

Received Sept. 12, 1991; revision received April 16, 1992; accepted for publication April 27, 1992.

*Graduate Student, Department of Aerospace Engineering. Student Member AIAA.
†Professor, Department of Aerospace Engineering.

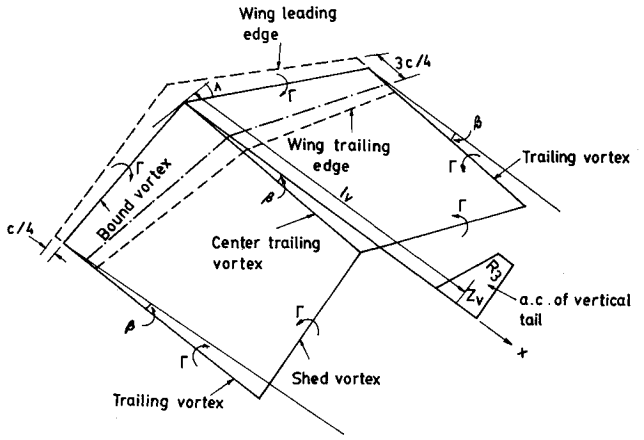

a) Vortex pattern of a sideslipping wing

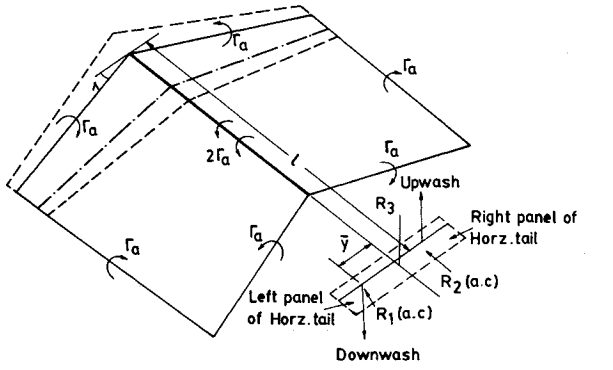

b) Asymmetric vortex pattern due to positive aileron input

Fig. 1 Simplified arrangement of a vortex system for a sideslipping wing and a wing with deflected ailerons.

effective angle-of-attack change caused by deflection of aileron surface on that panel. The vortices have the direction as shown in Fig. 1b and the same circulation strength of Γ_a as determined by the lift generated on each panel given by $C_{L_{\delta_a}}\delta_a/2$. Induced velocities were calculated at the aerodynamic center (a.c.) of the left panel (R_1) and right panel (R_2) of horizontal tail, and also at a.c. of vertical tail (R_3).

The trailing vortices in Fig. 1 are assumed to move in the plane of the wing and at one-half the freestream velocity.[1] Biot-Savart law can now be used to calculate induced velocities, and thereby, induced angles at the tail surfaces. It is also assumed that the total change in the induced angle at the tail surfaces can be obtained by superposition of the induced angles due to vortex system of Figs. 1a and 1b. Furthermore, any interference effects are considered unimportant in comparison to the individual effects.

Following the method of analysis of Ref. 6, indicial induced sidewash angle $\Delta\sigma_1$, for a unit step increase in sideslip angle β, was calculated at the a.c. of the vertical tail using Biot-Savart law for the vortex pattern in Fig. 1a, and then its accuracy improved by ensuring its correctness at the known steady-state conditions.[6] The expression for $\Delta\sigma_1$ so obtained was found to be long and complicated, and therefore, not in a suitable form for use in aircraft lateral equations of motion for parameter estimation. To that purpose, $\Delta\sigma_1$ was calculated for a few specific cases and after some trials the following form suitable for parameter estimation was obtained:

$$\Delta\sigma_1 = \left(\frac{d\sigma}{d\beta}\right)_{ss}\left[1 - D\exp\left(\frac{-2Eut^2}{c_r}\right) - \frac{F\tan\Lambda}{[(l_v/c_r) - G - (ut/2c_r)]^2 + (z_v H)^2}\right] \quad (1)$$

where $(d\sigma/d\beta)_{ss}$ can be estimated reasonably accurately from Refs. 8 and 9. The constants D to H are functions of wing and tail geometry and location, and can be evaluated by curve fitting Eq. (1) to the exact expression for $\Delta\sigma_1$ obtained from Biot-Savart law. Such curve-fitting, e.g., airplane with wings of sweep 0 and 30 deg, is shown in Fig. 2. It may be mentioned that Eq. (1) is an improvement over the one given in Ref. 6, since a more plausible vortex pattern has been used here for the case of swept wings. For unswept wings, however, the results from the present model differ only marginally from those obtained in Ref. 6.

Full-span positive aileron deflection is assumed to create the vortex system shown in Fig. 1b. Although the produced net lift remains unchanged, the strength of the vortices is governed by the wing and aileron geometry through the control derivative $C_{L_{\delta_a}}$. This vortex system will induce a sidewash at the vertical tail, and a downwash or upwash on the two panels of the horizontal stabilator. The induced sidewash and downwash/upwash are calculated as follows.

For the purpose of parameter estimation, the indicial sidewash angle $\Delta\sigma_2$ induced at the a.c. of the vertical tail, following a unit step increase in aileron input, was approximated by the following expression:

$$\Delta\sigma_2 = \left(\frac{d\sigma}{d\delta_a}\right)_{ss}\left[1 - I\exp\left(\frac{-2Jut^2 - 2Kl_v t}{c_r}\right)\right] \quad (2)$$

where constants I, J, K are evaluated by curve-fitting Eq. (2) to the exact expression for $\Delta\sigma_2$ obtained using Biot-Savart law to Fig. 1b. Since $(d\sigma/d\delta_a)_{ss}$ was not readily available, it was evaluated from the exact expression for $\Delta\sigma_2$ under steady-state conditions. Figure 3 shows the comparison of the actual curve (obtained using Biot-Savart law) and the approximate

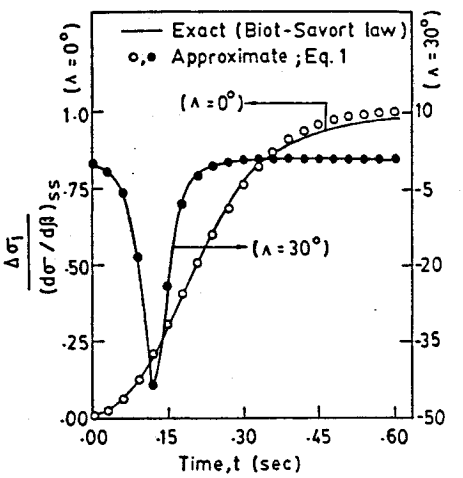

Fig. 2 Comparison of results from exact and approximate sidewash equations for sideslip.

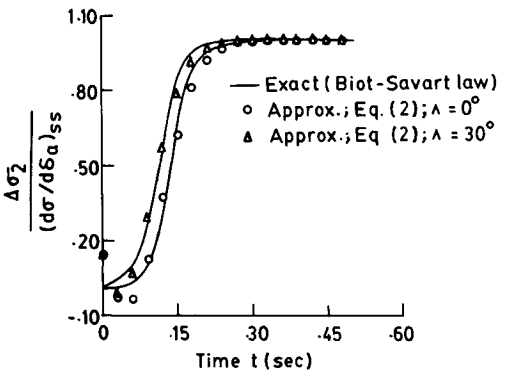

Fig. 3 Comparison of results from exact and approximate sidewash equations for aileron deflection.

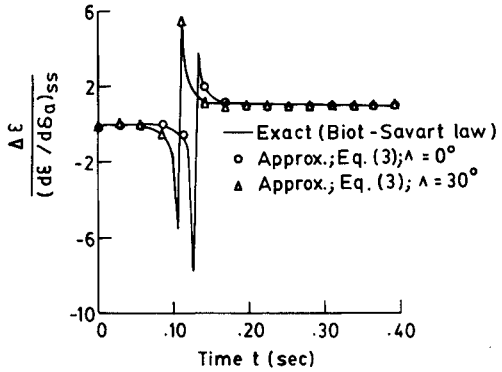

Fig. 4 Comparison of results from exact and approximate downwash equations.

curve [obtained from Eq. (2)] for $\Lambda = 0$ and 30 deg. Except for the region very near to the origin, the matching is reasonably good.

The asymmetric vortex system of Fig. 1b would induce a downwash on the left panel (looking from behind) and upwash on the right panel of the stabilator. Again, Biot-Savart law was used to calculate these induced angles at the a.c. of the left and right panels, and their correctness ensured for steady-state case. The expression so-obtained was then recast in the following form to render it amenable to laplace transform and thus suitable for parameter estimation in frequency-domain:

$$\Delta\varepsilon(t) = \left(\frac{d\varepsilon}{d\alpha}\right)_{l,ss} \alpha_\delta \left[1 - \frac{Lc_r}{(l - \bar{y}\tan\Lambda) - (ut/2) - c_r} - M\exp\left(-\frac{2Nut}{c_r}\right)\right] \tag{3}$$

where $(d\varepsilon/d\alpha)_{l,ss}$ can be estimated from Refs. 8 and 9, and the constants L, M, N are determined as before by curve-fitting Eq. (3) to the values of indicial downwash angle $\Delta\varepsilon$ obtained from Biot-Savart law. Figure 4 shows this curve fitting for $\Lambda = 0$ and 30 deg.

The other possible unsteady aerodynamic effects may arise from the lift buildup at the vertical and horizontal tails and such effects can be modeled by the indicial lift functions suggested in Refs. 6 and 7, e.g., the sideforce buildup at the vertical tail can be modeled by indicial side-force function

$$\Delta C_y = -a_v\left\{1 - y\exp\left[-\left(\frac{2zut}{c_v}\right)\right]\right\} \tag{4}$$

However, a brief study suggested that the buildup terms made a nonsignificant contribution to the response (in Fig. 6, to be discussed later). Therefore, in the model used for further analysis, such buildup terms were not considered and only the induced sidewash and downwash angles were retained as unsteady aerodynamic contributions.

Duhamel's integral was used to obtain induced angles and forces for arbitrary changes in $\beta(t)$ and $\delta_a(t)$

$$\sigma_1(t) = \int_0^t \Delta\sigma_1(t - \tau)\dot{\beta}(\tau)\,d\tau \tag{5}$$

$$\sigma_2(t) = \int_0^t \Delta\sigma_2(t - \tau)\dot{\delta}_a(\tau)\,d\tau \tag{6}$$

$$\varepsilon(t) = \int_0^t \Delta\varepsilon(t - \tau)\dot{\delta}_a(\tau)\,d\tau \tag{7}$$

$$C_y(t) = \int_0^t \Delta C_y(t - \tau)[\dot{\beta}(\tau) + \dot{\sigma}_1(\tau) + \dot{\sigma}_2(\tau)]\,d\tau \tag{8}$$

$$C_{L_t}(t) = \int_0^t \Delta C_{L_t}(t - \tau)[\dot{\alpha}(\tau) \pm \dot{\varepsilon}(\tau)]\,d\tau \tag{9}$$

where + and − signs are for the upwash on the right panel and downwash on the left panel of horizontal stabilator, respectively.

For parameter estimation it was found expedient to transform the above equations into the frequency-domain. Laplace transform of Eqs. (5–9) yields

$$\sigma_1(s) = \left(\frac{d\sigma}{d\beta}\right)_{ss}[1 - D_1(s)]\beta(s) \tag{10}$$

$$\sigma_2(s) = \left(\frac{d\sigma}{d\delta_a}\right)_{ss}[1 - D_2(s)]\delta_a(s) \tag{11}$$

$$\varepsilon(s) = \left(\frac{d\varepsilon}{d\alpha}\right)_{l,ss}[1 - D_3(s)]\delta_a(s) \tag{12}$$

$$C_y(s) = -a_v[\beta(s) + \sigma_1(s) + \sigma_2(s)] \tag{13}$$

$$C_{L_t}(s) = a_t[\alpha(s) \pm \varepsilon(s)] \tag{14}$$

where functions D_1 to D_3 are defined in the Appendix.

The coupled perturbed lateral equations of motion in the frequency domain can be written as

$$A\tilde{x} = B\tilde{u} \tag{15}$$

$$\tilde{z} = C\tilde{x} + \tilde{v} \tag{16}$$

where $\tilde{x}$, $\tilde{u}$, $\tilde{z}$, and $\tilde{v}$, are the state, control, output and measurement noise vectors, respectively. A and B are the system matrices and C is the observation matrix:

$$\tilde{x} = [\tilde{\beta}, \tilde{p}, \tilde{r}, \tilde{\phi}]^\top$$
$$\tilde{z} = [\tilde{\beta}, \tilde{p}, \tilde{r}, \tilde{a}_y]^\top$$
$$\tilde{u} = [\tilde{\delta}_r, \tilde{\delta}_a]^\top$$

The system matrices in Eqs. (15) and (16) are formulated as

$$A = \begin{bmatrix} j\omega - k_1\left[(C_{y_\beta})_{ss} + \frac{S_v}{S_w}P_1\right] & -k_2(C_{y_p})_{ss} & 1 - k_2(C_{y_r})_{ss} & -k_7 \\ -k_3[(C_{l_\beta})_{ss} + k_{10}P_1] & j\omega - k_4(C_{l_p})_{ss} & -k_4(C_{l_r})_{ss} & 0 \\ -k_5[(C_{n_\beta})_{ss} - k_{11}P_1] & -k_6(C_{n_p})_{ss} & j\omega - k_6(C_{n_r})_{ss} & 0 \\ 0 & -1 & 0 & j\omega \end{bmatrix}$$

$$B = \begin{bmatrix} k_1(C_{y_{\delta_r}})_{ss} & k_1[(C_{y_{\delta_a}})_{ss} - k_8P_2] \\ k_3(C_{l_{\delta_r}})_{ss} & k_3[(C_{l_{\delta_a}})_{ss} - k_{10}P_2 - k_9P_3] \\ k_5(C_{n_{\delta_r}})_{ss} & k_5[(C_{n_{\delta_a}})_{ss} + k_{11}P_2] \\ 0 & 0 \end{bmatrix}$$

$$C = \begin{bmatrix} 1 & 0 & 0 & 0 \\ 0 & 1 & 0 & 0 \\ 0 & 0 & 1 & 0 \\ 0 & 0 & 0 & 1 \\ j\omega/k_7 & 0 & 1/k_7 & -1 \end{bmatrix}$$

where

$$\tilde{P}_1 = a_v\left(\frac{d\sigma}{d\beta}\right)_{ss}\tilde{D}_1(j\omega)$$

$$\tilde{P}_2 = a_v\left(\frac{d\sigma}{d\delta_a}\right)_{ss}[1 - \tilde{D}_2(j\omega)]$$

$$\tilde{P}_3 = a_t\left(\frac{d\varepsilon}{d\alpha}\right)_{l,ss}\alpha_\delta[1 - \tilde{D}_3(j\omega)]$$

and constants k_1 to k_{11} are defined as

$$k_1 = \rho u S_w/2m \quad k_2 = \rho b S_w/4m \quad k_3 = \rho b S_w u^2/2I_x$$
$$k_4 = \rho u S_w b^2/4I_x \quad k_5 = \rho u^2 S_w b/2I_z \quad k_6 = \rho u S_w b^2/4I_z$$
$$k_7 = g/u \quad k_8 = S_v/S_w \quad k_9 = 2S_t\bar{y}/S_w b$$
$$k_{10} = S_v z_v/S_w b \quad k_{11} = S_v l_v/S_w b$$

All the stability and control derivatives C_{y_β}, C_{l_β}, . . . , $C_{n_{\delta_a}}$ represent the steady-state values of the parameters. For brevity of notation, the subscript "ss" has been dropped in further reference to the parameters.

Results and Discussion

Due to nonavailability of real flight data, an airplane similar to Navion used in Ref. 6 was considered for generating simulated flight data. The control inputs used are as shown in Fig. 5. To compare the relative contributions from time-lag effects and indicial load buildup on vertical and horizontal tails, the frequency response curves for yaw rate are shown in Fig. 6. As seen from the figure, the two responses with and without the load buildup terms are identical within the scale of the figure (of course, both responses include the time-lag effects). However, both of these responses show departure from the response without unsteady effects, and therefore, show the contribution of unsteady aerodynamics. In view of similar observations made for the other output variables, the load buildup terms were dropped from the equations of motion used for parameter estimation.

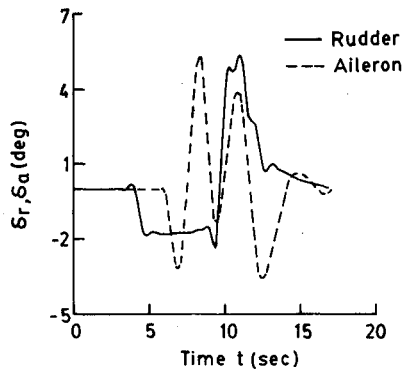

Fig. 5 Control input form used to generate simulated flight data.

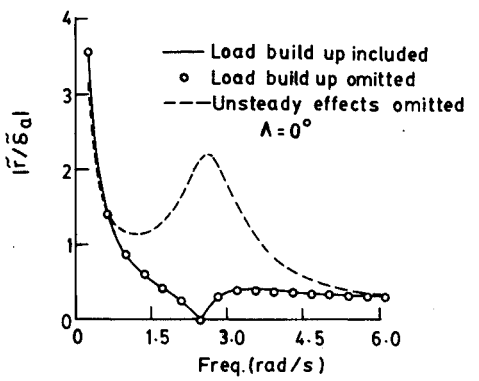

Fig. 6 Comparison of frequency response curves with load buildup included, load buildup omitted, and unsteady effects omitted.

The simulated data always contained the unsteady aerodynamic effects while three different models were used for parameter estimation: case I, model included all unsteady aerodynamic effects; case II, model omitted time-lag effects ($\tilde{D}_1 = \tilde{D}_2 = \tilde{D}_3 = 0$); and case III, model omitted any variation in steady-state vortex system

$$(\tilde{P}_1 = \tilde{P}_2 = \tilde{P}_3 = 0)$$

Results were obtained for case I for 0, 5, and 10% noise level. As expected, the parameters were well-estimated and Cramer-Rao bounds were low. The measured (simulated) and estimated responses matched well for all the observed variables.

Next, parameters were estimated for case II and case III for both $\Lambda = 0$ and 30 deg. The results for $\Lambda = 30$ deg are given in Table 1, along with those for case I for comparison. Absorption of time-lag effects results in equivalent parameters being estimated for case II, and thus shows variation from true values. The variation is further pronounced for case III, wherein all the unsteady aerodynamic contributions present in the flight data are absorbed in equivalent estimated parameters. Specifically, large changes in $C_{l_{\delta a}}$ and $C_{n_{\delta_a}}$ (sign change) for case III, and poor estimates of C_{n_p} for both case II and case III may be noted. Figure 7 compares the estimated responses for cases II and III with the measured response. The matching of responses for both cases II and III with measured response is good even though quite a few estimated parameters show significant difference from the true values. The following interpretation of the results given in Table 1 helps to explain this apparent anomaly.

Relatively large errors are observed in the aileron control derivatives $C_{y_{\delta a}}$, $C_{l_{\delta a}}$, $C_{n_{\delta a}}$, and in stability derivatives C_{l_r} and C_{n_r}. In the equations of motion with unsteady aerodynamics, the total aileron control derivatives as defined in matrix B of Eq. (15) may be represented by

$$C'_{y_{\delta_a}} = C_{y_{\delta_a}} - K_8 P_2 \tag{17a}$$

$$C'_{l_{\delta_a}} = C_{l_{\delta_a}} - K_{10} P_2 - K_9 P_3 \tag{17b}$$

$$C'_{n_{\delta_a}} = C_{n_{\delta_a}} + K_{11} P_2 \tag{17c}$$

Table 1 Comparison of estimated parameters for cases I, II, and III; $\Lambda = 30$ deg

Parameters	True value	Estimated values					
		Case I		Case II		Case III	
$-C_{y_\beta}$	0.3702	0.3702	(0)[a]	0.4003	(0.0128)[a]	0.3999	(0.0115)[a]
$-C_{y_p}$	0.0400	0.0400	(0)	0.2087	(0.0344)	0.1964	(0.0309)
$C_{y_{\delta r}}$	0.0970	0.0970	(0)	0.0856	(0.0086)	0.0880	(0.0078)
$C_{y_{\delta a}}$	0.0	0.0	(0)	0.0908	(0.0164)	−0.0362	(0.0147)
$-C_{l_\beta}$	0.2152	0.2152	(0)	0.2124	(0.0054)	0.2116	(0.0061)
$-C_{l_p}$	0.4540	0.4540	(0)	0.4652	(0.0129)	0.4661	(0.0146)
C_{l_r}	0.2550	0.2550	(0)	0.1281	(0.0110)	0.1407	(0.0126)
$C_{l_{\delta r}}$	0.0383	0.0383	(0)	0.0376	(0.0031)	0.0366	(0.0035)
$C_{l_{\delta a}}$	0.2590	0.2590	(0)	0.2533	(0.0059)	0.2396	(0.0068)
C_{n_β}	0.1488	0.1488	(0)	0.1481	(0.0007)	0.1476	(0.0008)
$-C_{n_p}$	0.0452	0.0452	(0)	0.0047	(0.0025)	0.0070	(0.0028)
$-C_{n_r}$	0.2700	0.2700	(0)	0.1432	(0.0034)	0.1462	(0.0038)
$-C_{n_{\delta r}}$	0.0720	0.0720	(0)	0.0714	(0.0010)	0.0721	(0.0011)
$-C_{n_{\delta a}}$	0.0250	0.0250	(0)	0.0415	(0.0012)	−0.0151	(0.0014)

[a]Cramer-Rao bounds.

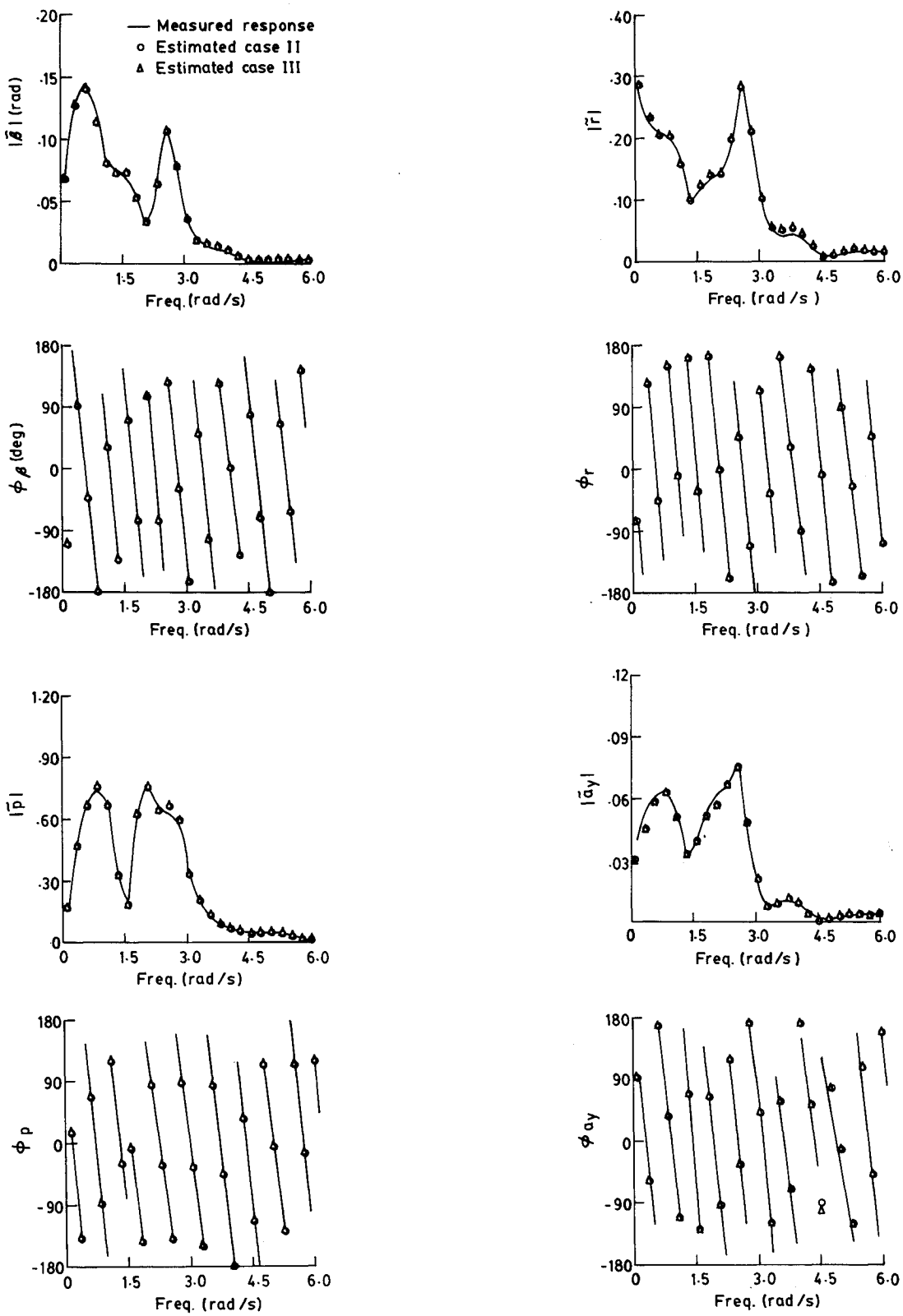

Fig. 7 Comparison of estimated response for case II and case III with measured response.

Table 2 Comparison of the true values of the equivalent derivatives with estimated values for cases II and III, $\Lambda = 30$ deg

Parameter	True value	Estimated	
		Case II	Case III
$C''_{y_{\delta a}}$	−0.1209	−0.0301	−0.0362
$C''_{l_{\delta a}}$	0.2440	0.2383	0.2396
$C''_{n_{\delta a}}$	0.0307	0.0142	0.0151

Table 3 Variation of estimated parameters with control input form for cases I, II, and III, Λ = 30 deg, noise level = 5%

Parameter	C_{y_β}	$C_{y_{\delta_r}}$	C_{n_β}	C_{l_r}	C_{n_r}	C_{l_p}	C_{n_p}	$C_{l_{\delta_a}}$	$C_{n_{\delta_a}}$
Change in									
Case I, %	0.01	0.02	0.05	0.00	0.04	0.00	0.11	0.03	0.12
Case II, %	11.7	13.5	8.40	8.10	9.90	7.60	78.9	2.40	22.1
Case III, %	11.5	11.6	4.10	15.7	6.60	9.10	82.6	4.30	44.4

If the vortex system due to aileron input were considered while the time-lag effect was neglected ($\tilde{D}_1 = \tilde{D}_2 = \tilde{D}_3 = 0$), the equivalent derivatives for case II can be defined from Eqs. (17) as

$$C''_{y_{\delta_a}} = C_{y_{\delta_a}} - K_8 a_v \left(\frac{d\sigma}{d\delta_a}\right)_{ss} \tag{18a}$$

$$C''_{l_{\delta_a}} = C_{l_{\delta_a}} - K_{10} a_v \left(\frac{d\sigma}{d\delta_a}\right)_{ss} - K_9 a_t \left(\frac{d\varepsilon}{d\alpha}\right)_{l,ss} \alpha_\delta \tag{18b}$$

$$C''_{n_{\delta_a}} = C_{n_{\delta_a}} + K_{11} a_v \left(\frac{d\sigma}{d\delta_a}\right)_{ss} \tag{18c}$$

Similarly for case III ($\tilde{P}_1 = \tilde{P}_2 = \tilde{P}_3 = 0$), the equivalent derivatives will simply be the steady-state derivatives:

$$C''_{y_{\delta_a}} = C_{y_{\delta_a}}, \quad C''_{l_{\delta_a}} = C_{l_{\delta_a}}, \quad \text{and} \quad C''_{n_{\delta_a}} = C_{n_{\delta_a}} \tag{19}$$

The values of total aileron control derivatives used for generating measured response are frequency-dependent as given by Eqs. (17). However, estimated parameters are the equivalent parameters as given by Eqs. (18) for case II and by Eq. (19) for case III. Thus, for a better comparison, true values of equivalent derivatives from Eqs. (18) were computed and compared with estimated equivalent values for case II and case III as shown in Table 2. It shows that the sign change observed earlier in case III for $C_{y_{\delta a}}$ and $C_{n_{\delta a}}$ is no longer present. Both true and estimated values of $C_{n_{\delta_a}}$ are positive. This seems to imply that the vortex pattern due to aileron deflection renders the equivalent $C_{n_{\delta a}}$ positive, and thereby, the estimated steady-state $C_{n_{\delta_a}}$ for case III also has positive sign after having absorbed the unsteady aerodynamic effects.

As discussed in Ref. 6, the other parameters C_{l_r} and C_{n_r} are most affected due to sideslipping phenomenon and consequent vortex system generated. Finally, a brief study was also carried out to see the relative importance of sidewash induced at the vertical tail and downwash at the horizontal tail. For the example airplane, sidewash effect due to vortex system for aileron deflection were more significant than the downwash effects. A large horizontal tail or a canard configuration may, however, lead to downwash effects being comparable to sidewash.

Queijo et al.[2] had suggested that the extracted parameters may show less variation for different control inputs when unsteady aerodynamics is included as compared to when it is not taken into account. To that purpose, many control input forms were used to generate simulated flight data and parameters estimated for cases I, II, and III. Percent change in estimated parameters for two different control input forms was calculated. Such changes for two control inputs are compared in Table 3. The large percentage variation for C_{n_p} seems to suggest that the parameter is highly sensitive to the control input form, and this explains poor estimates of it as mentioned earlier. The least percent change for all the parameters for case I seems to confirm that the unsteady aerodynamic modeling does reduce the dependence of estimated parameters on control input forms.

Conclusions

A simplified vortex model has been developed to account for unsteady aerodynamic effects due to aileron deflections and wing sideslipping motion. Computer-generated data with unsteady aerodynamic effects for an example airplane was utilized. To assess the effect of unsteady aerodynamics, parameters were estimated using two models, one including and other excluding (either fully or partially) unsteady aerodynamic effects. For the airplane considered, the results indicate that inclusion of unsteady effects does show significant difference in some of the parameters, particularly in aileron control derivatives. The inclusion of unsteady effects in estimation model helps to reduce the dependence of parameter estimates on control input forms.

Appendix

Expressions for functions D_1 to D_3 appearing in Eqs. (10–12) are as follows:

$$D_1(s) = s\left[\int_0^\infty De^{-at^2}e^{-st}\,dt + \int_0^\infty \frac{ge^{-st}}{(t-b)^2 + d^2}\,dt\right]$$

where

$$a = 2Eu/c_r \qquad b = 2c_r[(l_v/c_r) - G]/u$$

$$d = 2z_v Hc_r/u \qquad g = 4Fc_r^2 \tan\Lambda/u^2$$

and $s = j\omega$. Constants D, E, F, G, and H are determined from Eq. (1). The above integrals can be evaluated from standard tables of Refs. 10 and 11

$$\int_0^\infty e^{-at^2}e^{-st}\,dt = \frac{1}{2}\sqrt{\pi/a}\,\exp(s^2/4a)erfc(s/2\sqrt{a})$$

where *erfc* is the complementary error function[10]

$$\int_0^\infty \frac{e^{-st}}{(t-b)^2 + d^2}\,dt = \int_0^b \frac{e^{-st}}{(t-b)^2 + d^2}\,dt + \int_b^\infty \frac{e^{-st}}{(t-b)^2 + d^2}\,dt$$

$$\int_0^b \frac{e^{-st}}{(t-b)^2 + d^2}\,dt = \frac{je^{-bs}}{2d}\{e^x[E_1(x-bs) - E_1(x)]\}_{d\omega}^{-d\omega}$$

$$\int_b^\infty \frac{e^{-st}}{(t-b)^2 + d^2}\,dt = \frac{e^{-bs}}{d}\left\{\sin(sd)Ci(sd) - \cos(sd)\left[Si(sd) - \frac{\pi}{2}\right]\right\}$$

Here E_1, Si, and Ci are the exponential, sine and cosine integrals,[10] respectively

$$D_2(s) = (Is/2)\sqrt{\pi/f}\,\exp[(h+s)^2/4f]erfc[(h+s)/2\sqrt{f}]$$

where

$$f = 2Ju/c_r$$

$$h = 2Kl_v/c_r.$$

Constants I, J, and K are determined from Eq. (2)

$$D_3(s) = \frac{Ms}{s + (2Nu/c_r)} + \frac{2sLc_r}{u}\exp(-m)Ei(m)$$

where Ei is the exponential integral[10] and $m = 2s[1 - \bar{y} \tan \Lambda - c_r]/u$. Constants L, M, and N are defined in Eq. (3).

References

[1]Queijo, M. J., Wells, W. R., and Keskar, D. A., "Approximate Indicial Lift Function for Tapered Swept Wings in Incompressible Flow," NASA TP-1241, Aug. 1978.

[2]Queijo, M. J., Wells, W. R., and Keskar, D. A., "Inclusion of Unsteady Aerodynamics in Longitudinal Parameter Estimation from Flight Data," NASA TP 1536, Dec. 1979.

[3]Raisinghani, S. C., and Ghosh, A. K., "Parameter Estimation of an Augmented Airplane with Unsteady Aerodynamic Modelling," *Proceedings of the 17th International Symposium on Space Technology and Science*, Tokyo, Japan, May 20–25, 1990, pp. 699–706.

[4]Wells, W. R., Banda, S., and Quam, D. L., "Model for Unsteadiness in Lateral Dynamics for Use in Parameter Estimation," *Journal of Aircraft*, Vol. 17, No. 9, 1980, pp. 702–704.

[5]Raisinghani, S. C., and Singh, J., "Lateral Dynamics with Unsteady Aerodynamic Modelling for Parameter Estimation," 9th IFAC/IFORS Symposium of Identification and System Parameter Estimation, Budapest, Hungary, July 8–12, 1991.

[6]Singh, J., and Raisinghani, S. C., "Unsteady Aerodynamic Modelling for Aircraft Lateral Parameter Estimation," *Aeronautical Journal*, Vol. 95, March 1991, pp. 88–94.

[7]Wells, W. R., Banda, S., and Quam, D. L., "Aircraft Lateral Parameter Estimation from Flight Data with Unsteady Aerodynamic Modelling," *Proceedings of the 19th AIAA Aerospace Sciences Meeting*, St. Louis, MO, Jan. 12–15, 1981; see also AIAA Paper 81-0221, 1981.

[8]Roskam, J., *Methods for Estimating Stability and Control Derivatives for Conventional Subsonic Airplanes*, Roskam Aviation and Engineering Corp., 1973.

[9]Hoak, D. E., and Ellison, D. E., USAF Stability and Control DATCOM, Flight Control Div., Airforce Flight Dynamics Lab., Wright-Patterson AFB, OH, 1960, revised 1975.

[10]Abromowitz, M., and Stegun, I. A., *Handbook of Mathematical Functions with Formulas, Graphs and Mathematical Tables*, Dover, New York, 1965, pp. 228–237.

[11]Grobner, W., and Hofreiter, N., *Integraltafel*, Springer-Verlag, Win and Innsbruck, Austria, 1950, pp. 55–57.